

***In situ* photoemission study of collective electronic phase transition in VO₂-based heterostructures**

D. Shiga^{1,2,*}, S. Inoue¹, T. Kanda¹, N. Hasegawa¹, M. Kitamura², K. Horiba², K. Yoshimatsu¹,
A. F. Santander-Syro³, and H. Kumigashira^{1,2,*}

¹ *Institute of Multidisciplinary Research for Advanced Materials (IMRAM), Tohoku University, Sendai 980–8577, Japan*

² *Photon Factory, Institute of Materials Structure Science, High Energy Accelerator Research Organization (KEK), Tsukuba 305–0801, Japan*

³ *Institut des Sciences Moléculaires d'Orsay, Université Paris-Saclay, 91405 Orsay, France*

Abstract

We investigated the origin of collective electronic phase transitions induced at the heterointerface between monoclinic insulating (MI) VO₂ and rutile metallic (RM) electron-doped VO₂ layers using *in situ* soft x-ray photoelectron spectroscopy (SX PES) on nanoscale VO₂/V_{0.99}W_{0.01}O₂ (001)_R bilayers. Thanks to the surface sensitivity of SX PES, we determined the changes in the electronic structure and V-V dimerization in each constituent layer separately. The selective observation of the electronic and crystal structures in the upper VO₂ layer of the bilayer indicates that the MI-phase VO₂ layer undergoes a transition to the RM phase by forming the heterointerface. Detailed temperature-dependent measurements reveal that the RM-phase VO₂ undergoes a transition to the MI phase with a decrease in temperature, as in the case of a VO₂ single-layer film. Furthermore, during the temperature-induced phase transition in the VO₂ layer, the spectra are well described by an in-plane phase separation of the RM and MI phases. These results suggest that the interface-induced transition from the MI phase to the RM phase in the VO₂ layer of bilayers occurs as a collective phase transition derived from the static energy balance between the interfacial energy and the bulk free energies of the constituent layers.

*Correspondence authors: dshiga@tohoku.ac.jp, kumigashira@tohoku.ac.jp

I. INTRODUCTION

Vanadium dioxide (VO_2) shows an intriguing first-order metal-insulator transition (MIT) near room temperature that has been controversially discussed for over 60 years, in particular because both a structural transition and electron correlations contribute to it [1–21]. Across the MIT, the crystal and electronic structures change from a high-temperature rutile metallic (RM) phase to a low-temperature monoclinic insulating (MI) phase, concomitant with a dimerization of V atoms along the $[001]_R$ (c_R -axis) direction [2,3]. The MIT is also accompanied by a change in conductivity of several orders of magnitude and exhibits an ultrafast response to external stimuli. Thus, the MIT in VO_2 has become a central topic in condensed matter physics for its potential applications in Mottronics devices [22–28]. Further, this unusual phenomenon originating from the interplay of lattice dynamics and electron correlations provides a unique testbed to understand the physics of strongly correlated oxides.

The structural phase transition in VO_2 is characterized by the tilting and pairing of V ions, resulting in the collective dimerization of V ions along the $[001]_R$ direction in the MI phase [2,3]. Although the MIT that is concomitant with the collective V-V dimerization is reminiscent of the Peierls transition [4,5], the important role that strong electron correlations have in driving the MIT in VO_2 has also been evidenced from a large number of experimental and theoretical investigations [6,7]. Therefore, the mechanism of the MIT in VO_2 is now mainly understood as a cooperative Mott-Peierls transition [9–17].

This type of MIT in VO_2 has motivated researchers to control the electronic and structural phase transition by changing the delicate interplay between the electron correlations and the lattice via interfacial effects. Yajima *et al.* [29] have reported the occurrence of a collective MIT in bilayer structures composed of VO_2 layers with different MIT temperatures (T_{MITs}). The bilayer consists of a nondoped VO_2 layer with $T_{\text{MIT}} = 293$ K and an electron-doped (W-doped) VO_2 layer with slightly lower T_{MIT} of 257 K. It shows a collective (interlocked) transition at a certain critical layer thickness, while each layer undergoes the MIT at its respective T_{MIT} above the collective length, which corresponds to ~ 4.5 nm for each layer. In the collective MIT, the VO_2 layer undergoes a transition from insulator to metal by forming the interface with the electron-doped VO_2 . This collective transition is interpreted as originating from the static energy balance between the interfacial energy and the bulk free energies (the electronic and structural energies)

of the constituent layers. In this scenario (Scenario I), the collective phase transition of the VO₂ layer is interpreted as increased stability of the RM phase relative to the MI phase to avoid the cost of interfacial energy between the different phases.

In the collective MIT derived from the static energy balance, the MIT in the VO₂ layer should be the original transition from the MI to the RM phase. Namely, the metallic state in the VO₂ layer should be in the RM phase. However, Lee *et al.* [30] have recently suggested the possibility of realizing a new “monoclinic metallic (MM)” phase in the VO₂ layer of the bilayer structure. In this alternative scenario (Scenario II), an isostructural MI-MM phase transition, namely, a pure electronic phase transition without any structural transition, occurs in the VO₂ layer adjacent to the electron-doped VO₂ layer, although the doped layer maintains the RM phase.

To verify which of the two metallic states [RM phase (Scenario I) or MM phase (Scenario II)] is realized in the VO₂ layer, it is crucial to observe the electronic and crystal structures in each constituent layer separately. Against this background, in this study, we employed surface-sensitive photoemission spectroscopy (PES) and x-ray absorption spectroscopy (XAS) measurements in the soft-x-ray region to investigate the change in the electronic and crystal (characteristic V-V dimer) structures in the top VO₂ layer of VO₂/V_{0.99}W_{0.01}O₂ (W:VO₂) (001)_R bilayer structures. Thanks to a sufficiently shallow probing depth (1.5–2 nm) compared to each layer thickness (4.5 nm) in both spectroscopic measurements [15], information on the electronic and crystal structures of the upper VO₂ layer was selectively extracted. The PES and XAS spectra exhibited remarkable changes associated with phase transition in the upper VO₂ layers: (1) The upper VO₂ layer exhibits almost the same spectral behavior across the MIT as that of a VO₂ single-layer film, whereas its T_{MIT} is slightly lower than that of the single-layer film. (2) In the metallic states of the upper VO₂ layer, there is no indication of the V-V dimerization. (3) During the temperature-induced phase transition, both the PES and XAS spectra are described by a linear combination of the RM and MI phases, indicating the occurrence of an in-plane phase separation. These results strongly suggest that the upper VO₂ layer undergoes a collective transition from the MI to the RM phase by forming the heterointerface with the electron-doped VO₂ layer and that the MM phase does not emerge in the present VO₂/W:VO₂ (001)_R heterostructures. The occurrence of the phase transition from the MI to the RM phase in the VO₂ upper layers suggests that the collective phase transition originates from the static energy balance between the interfacial energy and the bulk free energies of the constituent layers (Scenario I).

II. EXPERIMENT

The $\text{VO}_2/\text{V}_{0.99}\text{W}_{0.01}\text{O}_2$ heterostructures were fabricated on the (001) surface of 0.05 wt% Nb-doped rutile- TiO_2 substrates in a pulsed-laser deposition (PLD) chamber connected to an *in situ* PES system at BL-2A MUSASHI of the Photon Factory, KEK [15–17,31,32]. Sintered pellets with appropriate compositions of V_2O_5 and $\text{V}_{1.98}\text{W}_{0.02}\text{O}_5$ were used as PLD ablation targets. Each layer was grown at a rate of 0.02 nm s^{-1} , as estimated from the Laue fringes in x-ray diffraction (XRD) patterns of a corresponding single-layer film. The growth conditions for each layer are described in detail elsewhere, and the characterization of the heterostructures is given in Supplemental Material [33]. During the deposition, the substrate temperature was maintained at $400 \text{ }^\circ\text{C}$, and the oxygen pressure was maintained at 10 mTorr. The thicknesses of the deposited VO_2 and $\text{W}:\text{VO}_2$ layers, as well as those of the VO_2 and $\text{W}:\text{VO}_2$ single-layer films, were precisely controlled by deposition time. The surface structures and cleanness of the heterostructures were confirmed via reflection high-energy electron diffraction and core-level photoemission measurements, respectively.

The surface morphologies of the measured heterostructures and single-layer films were analyzed via atomic force microscopy in air (see Fig. S1 in Supplemental Material [33]). The epitaxial relationship and crystalline quality were characterized by XRD, confirming the coherent growth of each layer. A sharp diffraction pattern with well-defined Laue fringes was observed, indicating the high quality of the heterostructures, i.e., homogeneously coherent films with atomically flat surfaces and interfaces (see Fig. S2 in Supplemental Material [33]). All bilayer structures were fabricated under the same conditions as previously reported bilayer structures [29], wherein chemically abrupt interfaces formed. The sheet conductance was measured using the standard four-probe method with a temperature ramp rate of 10 mK s^{-1} .

PES measurements were performed *in situ* with the use of a VG-Scienta SES-2002 analyzer with a total energy resolution of 120 meV at a photon energy of 700 eV. The vacuum transferring of the grown samples was necessary to prevent the overoxidation of the surface layer [15–17]. The XAS spectra were also measured *in situ* with linearly polarized light via the measurement of the sample drain current. For linear dichroism measurement of oxygen *K*-edge XAS (*O K* XAS), we acquired the XAS spectra at angles $\theta = 0^\circ$ and 60° between the $[100]_R$ direction and the polarization vector \mathbf{E} while maintaining a fixed angle between the direction normal to the interfaces and the incident light (see Fig. S3 in Supplemental Material [33]). Here, we emphasize

that the present O *K* XAS measurement is also surface sensitive; its probing depth is estimated to be almost identical to that of the present soft x-ray PES measurements (1.5–2 nm) (see Fig. S4 in Supplemental Material [33]). Therefore, both the PES and XAS spectra reflect the information from almost the same surface region of the top VO₂ layers. The Fermi energy (E_F) of each sample was determined by the measurement of a gold film that was electrically connected to the sample. As it is common knowledge that VO₂ exhibits an insulator-to-metal transition upon irradiation by light [36], we paid particular attention to the possible spectral changes induced by light irradiation (see Fig. S5 in Supplemental Material [33]). The stoichiometry of the constituent layers was carefully characterized by analyzing the relative intensities of the V-2*p* and -3*p*, O-1*s*, and W-4*f* core levels, confirming that the cation composition of the samples was the same as that of the PLD ablation targets. We carefully carried out temperature-dependent PES and XAS measurements by confirming that the spectral changes with temperature were saturated (hysteresis effects [11,29,34,40] were no longer present). Furthermore, the sample temperature was maintained at 320 K for half an hour before measuring, and then the measurements were performed only upon cooling to avoid the possible hysteresis effect (see Fig. S6 in Supplemental Material [33]).

III. RESULTS & DISCUSSION

Before discussing the PES spectra, we provide evidence that the prepared bilayers show essentially the same properties as those in the previous report [29]. Figure 1 shows the temperature dependence of sheet conductivity σ_{Sheet} upon cooling for VO₂ (4.5 nm)/W:VO₂ (4.5 nm) and VO₂ (6.5 nm)/W:VO₂ (6.5 nm) bilayers, together with that for 9-nm VO₂ and W:VO₂ single-layer films. For the single-layer films, the $\sigma_{\text{Sheet}}-T$ curve steeply changes across the MIT [15,16,40,41], as reported previously [29]. The corresponding T_{MIT} on the cooling process ($T_{\text{MIT}}^{\text{Cooling}}$), which is defined as the inflection point of each $\log_{10}\sigma_{\text{Sheet}}-T$ curve, is determined to be 286 K and 261 K for the VO₂ and W:VO₂ single-layer films, respectively. The values are in excellent agreement with the previous reports on epitaxial films coherently grown on TiO₂(001) substrates, guaranteeing almost the same qualities of the present films as those of the previous ones [15,16,27,29,34,40]. For the bilayers, two separate transitions are observed, reflecting the original $T_{\text{MIT}}^{\text{Cooling}}$ of constituent layers. This result suggests that the constituent layers behave independently despite the layered structure, although the $T_{\text{MIT}}^{\text{Cooling}}$ corresponding to the VO₂ layer is

slightly lower. In contrast, the two transitions seem to merge at 4.5-nm bilayers, reflecting the occurrence of the collective transition throughout the whole bilayer structure in the temperature range of 260–275 K. The observed layer-thickness dependence is in good agreement with that in the previous study [29], indicating the achievement of essentially the same properties in the present bilayers.

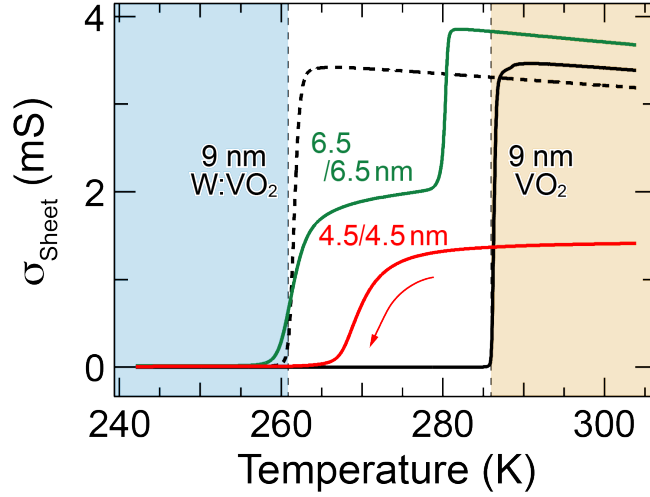


FIG. 1. Temperature dependence of σ_{Sheet} upon cooling for VO_2 (4.5 nm)/ W:VO_2 (4.5 nm) bilayer (red curve) and VO_2 (6.5 nm)/ W:VO_2 (6.5 nm) bilayer (green curve), together with that of 9-nm VO_2 and W:VO_2 single-layer films (solid and dashed black curves, respectively). Vertical dashed lines indicate $T_{\text{MIT}}^{\text{Cooling}}$ of the VO_2 and electron-doped W:VO_2 single-layer films (286 and 261 K, respectively). Here, $T_{\text{MIT}}^{\text{Cooling}}$ is defined as the inflection point in the $\log_{10}\sigma_{\text{Sheet}}-T$ curve in the cooling process (see text in more detail). The 6.5-nm bilayer exhibits two-separate transitions, indicating that the upper and lower layers undergo MIT separately. In contrast, the 4.5-nm bilayer shows a single transition, indicating the occurrence of the collective transition in the temperature range of 260–275 K. Note that the behaviors are essentially the same as the previous reports, guaranteeing the comparable quality of the single-layer films and bilayers in the present study [29].

To see the behavior of the collective phase transition in more detail, we present the temperature dependence of the sheet resistance R_{Sheet} in Fig. 2, alongside reference data of VO_2 and W:VO_2 single-layer films. The 4.5-nm bilayer exhibits a single-step MIT at $T_{\text{MIT}}^{\text{Cooling}} \sim 267$ K, in sharp contrast to the two-step MIT in the 6.5-nm bilayer (see Fig. 1). Furthermore, the transition is

relatively broad in comparison with the abrupt change across the MIT in the single-layer films, implying a complicated interplay between different phases in the two layers.

According to the previous studies [29,30], the complicated behaviors may be classified into four temperature regions A – D , as schematically illustrated in the upper panel of Fig. 2. At temperature A , both layers are in the RM phase, while at temperature D both layers are in the MI phase, since at those temperatures the original VO_2 and W:VO_2 layers are in the same corresponding RM or MI phases. Meanwhile, the upper VO_2 layer shows metallic behavior at temperature B as a result of the collective phase transition, although the VO_2 (W:VO_2) layer should be the MI (RM) phase in the case that each of the layers behaves independently as in the 6.5-nm bilayer. In other words, the VO_2 layer exhibits an insulator-to-metal transition by forming the interface with the electron-doped VO_2 with lower T_{MIT} . For Scenarios I and II, the possible metallic phase that emerged at B due to the corrective interface-induced phase transition is RM and MM, respectively. With decreasing the temperature, the metallic phase eventually exhibits a temperature-induced MIT around temperature C . As a result, the T_{MIT} of the VO_2 (W:VO_2) layer is suppressed (enhanced) owing to the proximity effect between the two layers.

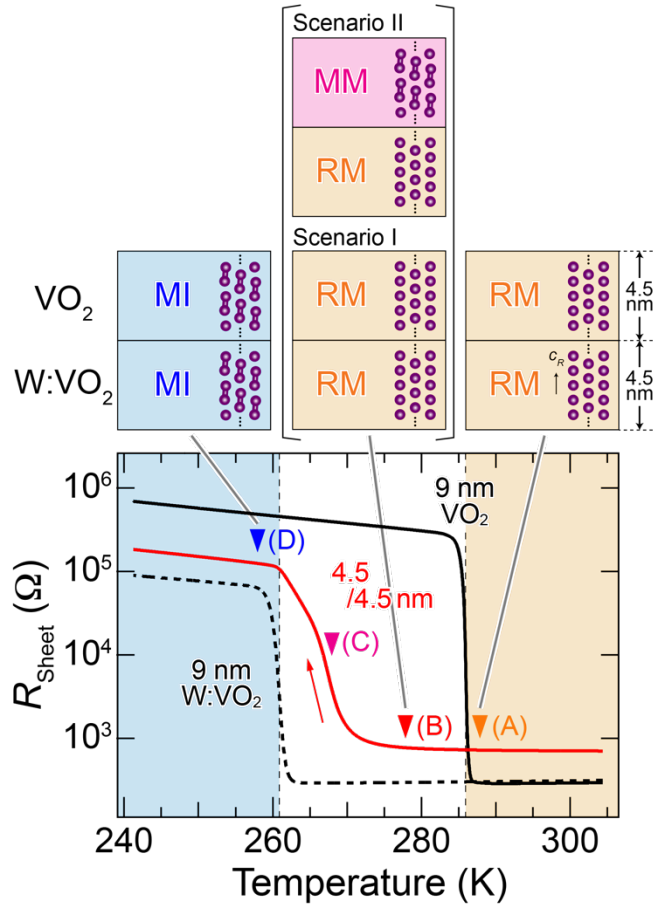


FIG. 2. Temperature dependence of R_{Sheet} measured upon cooling for VO_2 (4.5 nm)/ W:VO_2 (4.5 nm) bilayer (solid red curve), along with those of 9-nm VO_2 and W:VO_2 single-layer films (solid and dashed black curves, respectively). Vertical dashed lines indicate $T_{\text{MIT}}^{\text{Cooling}}$ of the VO_2 and W:VO_2 single-layer films (286 and 261 K, respectively), while colored solid triangles indicate the spectroscopic measurement points (A–D). The upper panel shows the schematic illustration for the expected electronic phases of the bilayer at temperatures A, B, and D. At temperature B, the two possible metallic phases of the upper VO_2 layer based on Scenarios I (interface-induced collective phase transition from MI to RM [29]) and II (isostructural interface-induced collective phase transition from MI to MM [30]) are presented. MI, RM, and MM denote the monoclinic insulating, rutile metallic, and monoclinic metallic phases, respectively.

To identify the metallic phase at temperature B, we measured the changes in the electronic structures and V-V dimerization in the upper VO_2 layer selectively through PES measurements. Figure 3(a) shows the valence-band spectra measured upon cooling at temperatures A–D for the

VO₂ (4.5 nm)/W:VO₂ (4.5 nm) bilayers grown on Nb:TiO₂ (001) substrates, in addition to those of VO₂ single-layer films in the MI and RM phases as references. Owing to the surface sensitivity of soft-x-ray PES, the spectra mostly reflect the electronic structure of the top 4.5-nm VO₂ layers, as schematically illustrated in the inset, since the probing depth of the present PES is 1.5–2 nm [15,33]. The spectra contain two main features: structures derived from O 2*p* states at binding energies of 3–10 eV, and peaks derived from the V 3*d* states near E_F . The spectra of the bilayer (i.e., the top VO₂ layer) exhibit the characteristic features of the MIT in VO₂ films [11,15–17,42–44]: the spectrum near E_F at temperature *A* consists of a sharp coherent peak at E_F and a weak broad satellite around 1.2 eV. Meanwhile, the spectrum at temperature *D* shows a single peak around 0.8 eV, corresponding to the formation of an energy gap at E_F .

For the upper VO₂ of the bilayer structure, the valence-band spectra at temperatures *A* and *D* are almost exactly the same as those of the VO₂ single-layer films in the RM and MI phases, respectively. At temperature *B* where the VO₂ layer changes from the original MI phase to the metallic phase (RM in Scenario I or MM in Scenario II) by forming the heterointerface (see Fig. 2), the spectra exhibit the features representative of the RM phase of the VO₂ single-layer film. In fact, the spectrum at temperature *B* is identical to the spectrum at temperature *A* (RM phase) within the experimental error, suggesting the occurrence of the MI-to-RM transition by forming the interface with the W:VO₂ layer. The metallic state eventually exhibits the transition to the MI phase at temperature *D* through certain complicated phenomena around temperature *C* (see Fig. 2). Furthermore, focusing on the O 2*p* states, we observe dramatic changes across the temperature-dependent MIT. For VO₂ films, these changes are attributed to the structural changes (V-V dimerization) concomitant with the MIT in VO₂ [11,15–17], strongly suggesting the occurrence of temperature-induced structural transition from the RM phase (temperatures *A* and *B*) to the MI phase (temperature *D*) in the upper VO₂ layer.

To verify the occurrence of the structural transition across the interface-induced MIT at temperature *B*, we measured, as shown in Fig. 3(b), the polarization dependence of O *K* XAS, which has been previously used as an indicator of V-V dimerization. The O *K* XAS probes the unoccupied O 2*p* partial density of states that are mixed with the unoccupied V 3*d* states and is thus complementary to PES for investigating the electronic structures of conduction bands. Because the V-V dimerization in the MI phase splits the half-filled $d_{||}$ state into occupied $d_{||}$ and unoccupied $d_{||}^*$ states, an additional peak corresponding to the $d_{||}^*$ states appears in the XAS spectra

only for the MI phase [3,11,32,45–47]. Moreover, owing to strict dipole selection rules, the additional d_{\parallel}^* states only appear in the spectra acquired with \mathbf{E} parallel to the $[001]_R$ (c_R -axis) direction ($\mathbf{E} \parallel c_R$). From the assignments made in previous studies [11,45], the d_{\parallel}^* peak emerges at 530.4 eV in the MI phase (temperature D) measured with the $\mathbf{E} \parallel c_R$ geometry, whereas it disappears in the RM one (temperature A). The identification of the d_{\parallel}^* states was further confirmed by the linear dichroism of the XAS spectra: the additional d_{\parallel}^* peak in the MI phase disappeared for the spectrum taken with $\mathbf{E} \perp c_R$ (see Fig. S3 in Supplemental Material [33]). Thus, the existence of the d_{\parallel}^* peak in the spectra with the $\mathbf{E} \parallel c_R$ geometry can be used as a fingerprint of the V-V dimerization in VO₂ [3,11,45,46].

Figure 3(b) shows the temperature dependence of *in situ* O *K* XAS spectra upon cooling acquired with $\mathbf{E} \parallel c_R$ of the bilayers. It should be noted that since the probing depth of the present XAS measurements is comparable to the PES measurements (Fig. S4 in Supplemental Material [33]), both spectra reflect information on the top 4.5-nm VO₂ layers [see the inset of Fig. 3(a)]. The spectra for the upper VO₂ layer show the RM and MI nature at temperatures A and D , respectively, as in the case of VO₂ single-layer films. In addition, the spectral shapes at the two temperatures A (RM) and B are almost identical, and no detectable d_{\parallel}^* state is observed, indicating the absence of V-V dimerization at temperature B . The selective observation of the electronic and crystal structures indicates that the upper VO₂ layer undergoes the transition from the MI to the RM phase by forming the heterointerface (Scenario I).

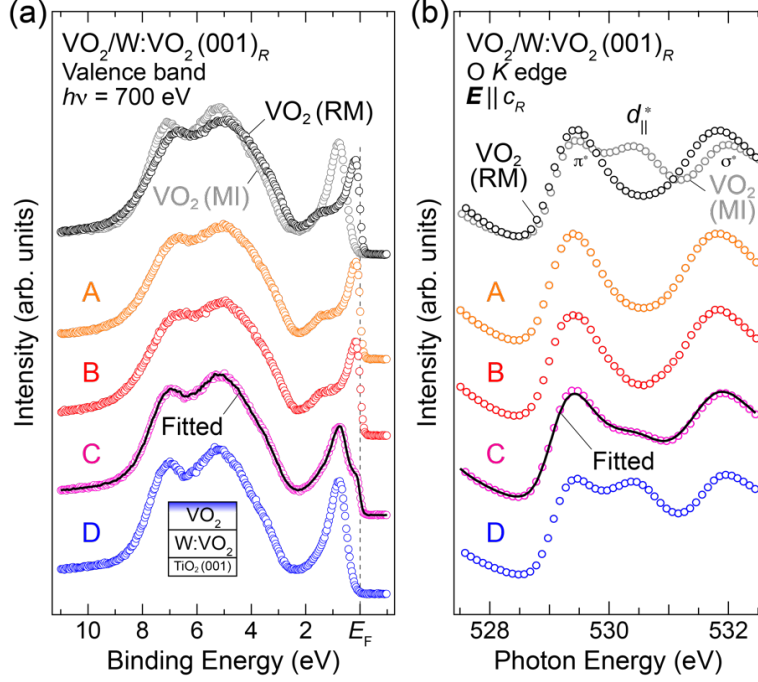


FIG. 3. Temperature dependence of *in situ* (a) valence-band spectra and (b) O *K* XAS spectra acquired with the $E \parallel c_R$ geometry [33] measured upon cooling for VO_2 (4.5 nm)/ W:VO_2 (4.5 nm) bilayers, together with a VO_2 film ($T_{\text{MIT}}^{\text{cooling}} = 286$ K) measured at its RM and MI phases as references. The measured temperatures of *A*, *B*, *C*, and *D* are shown in Fig. 2. For spectra *C*, the fitted result by the linear combination of the RM (*A*) and MI (*D*) phases [Eq. (1)] is overlaid by a black solid curve. Note that since the probing depth of the present (a) PES and (b) XAS measurements are comparable (1.5–2 nm [15,33]), both spectra reflect information on the top VO_2 layers, as schematically illustrated in the inset in (a). The spectra at temperature *B* are almost the same as those of a VO_2 film in the RM phase, as well as those at temperature *A*, indicating that the upper VO_2 layer undergoes the transition from MI to RM by forming the heterointerface.

In the $R_{\text{Sheet}}-T$ curve in Fig. 2, the temperature width of the collective MIT for the 4.5-nm $\text{VO}_2/\text{W:VO}_2$ bilayer is much broader than that of the original VO_2 and W:VO_2 single-layer films. Such broadening was also observed in the previous bilayers [29] as well as the VO_2 films grown on TiO_2 (110) substrates [36,48,49], implying the occurrence of some in-plane phase separation characteristic of VO_2 nanostructures. To shed light on the phenomena, we measured the PES and XAS spectra at temperature *C*, as shown in Fig. 3. The valence-band spectra at temperature *C* near E_F exhibit the peak at 0.8 eV, the same binding energy of spectra *D* corresponding to the MI

phase, and an additional structure at E_F indicative of metallic behavior. Upon closer inspection, spectra C appear to be an average of the spectra measured at temperatures A (RM phase) and D (MI phase). In general, in the case of phase separation, as the size of the soft-x-ray light spot used in the present PES and XAS experiments is much larger than the typical size of the phase domains, the measured spectrum is described by a linear combination of the spectra of each phase. Thus, we fit the spectra $I(\alpha)$ using the following equation [17,50]:

$$I(\alpha) = \alpha I_{\text{RM}} + (1 - \alpha) I_{\text{MI}}, \quad (1)$$

where α is the fraction of the RM phase, and I_{RM} and I_{MI} are the spectra of the RM phase (spectra A) and MI phase (spectra D), respectively. As can be seen at temperature C , both the PES and XAS spectra are almost perfectly described by the linear combination of the spectra for A (RM phase) and D (MI phase) with $\alpha = 0.4\text{--}0.5$. These results indicate that a phase separation of the RM and MI phases occurs in the upper VO_2 layer of the $\text{VO}_2/\text{W}:\text{VO}_2$ bilayer structure.

To investigate the phase-separation behavior in more detail, we measured the detailed temperature dependence of the PES and XAS spectra across the MIT and fitted them using Eq. (1), as shown in Fig. 4. As can be seen in Figs. 4(a) and 4(b), all the spectra during the phase transition are well described by the linear combination. The estimated values of α are plotted as a function of measured temperature in Fig. 4(c), together with the corresponding σ_{Sheet} (Fig. 1). Although the electrical conductance in the case of phase separation must be considered in terms of a percolation model, the good agreement between the σ_{Sheet} and α values suggests that the complex behavior across the MIT in the bilayer can be attributed to the phase separation. Furthermore, considering the difference in probing depth between these two types of measurements (soft-x-ray spectroscopies are sensitive to the top VO_2 layer, while resistivity measurement probes the entire bilayer), it is likely that the phase domain structures of the upper and lower layers in the bilayers are the same, and the bilayers undergo the collective phase transition. In such a case where the separation of the RM and MI phases occurs, it may appear that the MM phase emerges. Therefore, it is important to investigate the electronic and V-V dimer structures of each layer selectively using spectroscopic techniques that can probe only specific regions, as in this study.

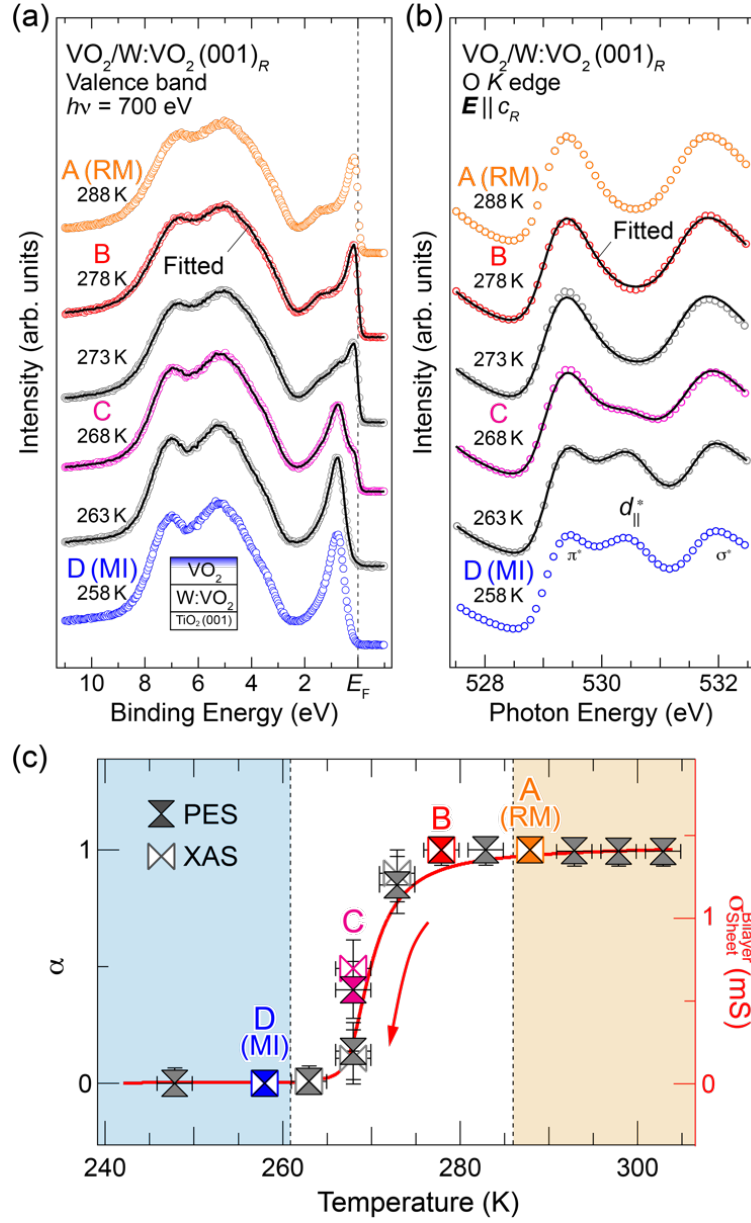


FIG. 4. Temperature dependence of *in situ* (a) valence-band and (b) O K XAS spectra measured near T_{MIT} upon cooling for VO_2 (4.5 nm)/ $\text{W}:\text{VO}_2$ (4.5 nm) bilayers. Note that the spectra mostly reflect the electronic structure of the upper VO_2 layer owing to the surface sensitivity of the present spectroscopic measurements. The fitted results by the linear combination of the RM (A) and the MI (D) phases [Eq. (1)] are overlaid on respective spectra. The spectra are almost perfectly described by the linear combination. (c) Plot of α as a function of temperature. The σ_{Sheet} of the bilayer (Fig. 1) is overlaid as a red curve for comparison.

The selective observation of the electronic and crystal structures of the constituent layers in the bilayers indicates that the upper VO₂ layer undergoes the transition from the MI to the RM phase by forming the heterointerface between VO₂ and W:VO₂ layers. However, it should be bear in mind that the present study does not eliminate the possibility of the emergence of the MM phase in VO₂-based bilayer structures. In comparison to the previous results of Lee *et al.* [30], there are several differences from the bilayers examined here: the difference (7 K) of T_{MIT} between constituent layers is much smaller than that in the present case (25 K), and electrons are doped by oxygen vacancies (VO_{2- δ}). The significantly smaller difference in T_{MIT} reflects a closer proximity between the electronic and structural energies of constituent layers, which may induce the emergence of the new equilibrium MM phase in the VO₂/VO_{2- δ} bilayer [30]. Furthermore, in chemically doped VO₂, the V-V dimer structure is known to change significantly depending on the type and concentration of the dopant, resulting in the complicated electronic phase diagram [34,51,52]. Therefore, the resultant complicated static energy balance between the interfacial energy and the bulk free energies of constituent layers may lead to the emergence of the MM phase in certain conditions. To gain a better understanding of the interface-induced collective phenomena occurring in the VO₂-based bilayers, further systematic investigations are required. In particular, investigations of the more detailed dopant and layer-thickness dependencies are necessary. Also, further theoretical works that adequately treat these effects will be necessary to examine the possibility of a new electronic phase in the bilayers.

V. CONCLUSION

We performed *in situ* PES and XAS measurements on VO₂/W:VO₂ bilayers to investigate the change in the electronic structure and characteristic V-V dimerization across the collective phase transition induced at the heterointerface between the MI-phase VO₂ and RM-phase W:VO₂ layers. Thanks to the surface sensitivity of PES and XAS in the soft-x-ray region, we extracted the changes in the top VO₂ layer separately. The spectra exhibited remarkable change associated with the collective phase transition: (1) The upper VO₂ layer exhibits almost the same spectral behavior across the MIT as that of a VO₂ single-layer film, whereas its T_{MIT} is slightly lower than that of the single-layer film. (2) In the metallic states of the upper VO₂ layer, there is no indication of the V-V dimerization. (3) During the phase transition, both the PES and XAS spectra are described by a linear combination of the RM and MI phases, indicating the occurrence of in-plane phase separation. These results strongly suggest that the upper VO₂ layer undergoes the collective transition from the MI to the RM phase by forming the heterointerface with the electron-doped VO₂ layer. The occurrence of the phase transition from the MI to RM phase in the VO₂ upper layers suggests that the collective phase transition originates from the static energy balance between the interface energy and the bulk free energies of the constituent layers.

ACKNOWLEDGMENTS

The authors are very grateful to T. Yajima, S. Biermann, and M. J. Rozenberg for our helpful discussions. This work was financially supported by a Grant-in-Aid for Scientific Research (Nos. 20KK0117, 21K20498, 22H01947, 22H01948, and 23H00263) from the Japan Society for the Promotion of Science (JSPS), CREST (JPMJCR18T1) from the Japan Science and Technology Agency (JST), and MEXT Program: Data Creation and Utilization Type Material Research and Development Project (Grant No. JPMXP1122683430). S.I. and T.K. acknowledges the financial support from the Division for Interdisciplinary Advanced Research and Education at Tohoku University. N.H. acknowledges the financial support from the Chemistry Personnel Cultivation Program of the Japan Chemical Industry Association. The work performed at KEK-PF was approved by the Program Advisory Committee (proposal Nos. 2019T004, 2022G675, 2021S2-002, and 2024S2-003) at the Institute of Materials Structure Science, KEK.

REFERENCES

- [1] F. J. Morin, *Phys. Rev. Lett.* **3**, 34 (1959).
- [2] N. F. Mott, *Rev. Mod. Phys.* **40**, 677 (1968).
- [3] J. B. Goodenough, *J. Solid State Chem.* **3**, 490 (1971).
- [4] D. Adler and H. Brooks, *Phys. Rev.* **155**, 826 (1967).
- [5] R. M. Wentzcovitch, W. W. Schulz, and P. B. Allen, *Phys. Rev. Lett.* **72**, 3389 (1994).
- [6] A. Zylbersztejn and N. F. Mott, *Phys. Rev. B* **11**, 4383 (1975).
- [7] T. M. Rice, H. Launois, and J. P. Pouget, *Phys. Rev. Lett.* **73**, 3042 (1994).
- [8] M. Imada, A. Fujimori, and Y. Tokura, *Rev. Mod. Phys.* **70**, 1039 (1998).
- [9] S. Biermann, A. Poteryaev, A. I. Lichtenstein, and A. Georges, *Phys. Rev. Lett.* **94**, 026404 (2005).
- [10] M. W. Haverkort, Z. Hu, A. Tanaka, W. Reichelt, S. V. Streltsov, M. A. Korotin, V. I. Anisimov, H. H. Hsieh, H.-J. Lin, C. T. Chen, D. I. Khomskii, and L. H. Tjeng, *Phys. Rev. Lett.* **95**, 196404 (2005).
- [11] T. C. Koethe, Z. Hu, M. W. Haverkort, C. Schüßler-Langeheine, F. Venturini, N. B. Brookes, O. Tjernberg, W. Reichelt, H. H. Hsieh, H.-J. Lin, C. T. Chen, and L. H. Tjeng, *Phys. Rev. Lett.* **97**, 116402 (2006).
- [12] M. M. Qazilbash, M. Brehm, B.-G. Chae, P.-C. Ho, G. O. Andreev, B.-J. Kim, S. J. Yun, A. V. Balatsky, M. B. Maple, F. Keilmann, H.-T. Kim, and D. N. Basov, *Science* **318**, 1750 (2007).
- [13] J. M. Tomczak, F. Aryasetiawan, and S. Biermann, *Phys. Rev. B* **78**, 115103 (2008).
- [14] M. M. Qazilbash, A. Tripathi, A. A. Schafgans, B.-J. Kim, H.-T. Kim, Z. Cai, M. V. Holt, J. M. Maser, F. Keilmann, O. G. Shpyrko, and D. N. Basov, *Phys. Rev. B* **83**, 165108 (2011).
- [15] D. Shiga, B. E. Yang, N. Hasegawa, T. Kanda, R. Tokunaga, K. Yoshimatsu, R. Yukawa, M. Kitamura, K. Horiba, and H. Kumigashira, *Phys. Rev. B* **102**, 115114 (2020).
- [16] D. Shiga, M. Minohara, M. Kitamura, R. Yukawa, K. Horiba, and H. Kumigashira, *Phys. Rev. B* **99**, 125120 (2019).
- [17] D. Shiga, X. Cheng, T. T. Kim, T. Kanda, N. Hasegawa, M. Kitamura, K. Yoshimatsu, and H. Kumigashira, *Phys. Rev. B* **108**, 045112 (2023).
- [18] M. Marezio, D. B. McWhan, J. P. Remeika, and P. D. Dernier, *Phys. Rev. B* **5**, 2541 (1972).
- [19] J. B. Goodenough and H. Y-P. Hong, *Phys. Rev. B* **8**, 1323 (1973).
- [20] J. P. Pouget, H. Launois, T. M. Rice, P. Dernier, A. Gossard, G. Villeneuve, and P.

- Hagemmuller, *Phys. Rev. B* **10**, 1801 (1974).
- [21] J. P. Pouget, H. Launois, J. P. D'Haenens, P. Merenda, and T. M. Rice, *Phys. Rev. Lett.* **35**, 873 (1975).
- [22] C. H. Ahn, A. Bhattacharya, M. Di Ventura, J. N. Eckstein, C. D. Frisbie, M. E. Gershenson, A. M. Goldman, I. H. Inoue, J. Mannhart, A. J. Millis, A. F. Morpurgo, D. Natelson, and J.-M. Triscone, *Rev. Mod. Phys.* **78**, 1185 (2006).
- [23] H. Takagi and H. Y. Hwang, *Science* **327**, 1601 (2010).
- [24] M. Nakano, K. Shibuya, D. Okuyama, T. Hatano, S. Ono, M. Kawasaki, Y. Iwasa, and Y. Tokura, *Nature (London)* **487**, 459 (2012).
- [25] H. Ji, J. Wei, and D. Natelson, *Nano Lett.* **12**, 2988 (2012).
- [26] J. Jeong, N. Aetukuri, T. Graf, T. D. Schladt, M. G. Samant, and S. S. P. Parkin, *Science* **339**, 1402 (2013).
- [27] K. Shibuya and A. Sawa, *Adv. Electron. Mater.* **2**, 1500131 (2016).
- [28] T. Yajima, T. Nishimura, and A. Toriumi, *Nat. Commun.* **6**, 10104 (2015).
- [29] T. Yajima, T. Nishimura, and A. Toriumi, *Small* **13**, 1603113 (2017).
- [30] D. Lee, B. Chung, Y. Shi, G.-Y. Kim, N. Campbell, F. Xue, K. Song, S.-Y. Choi, J. P. Podkaminer, T. H. Kim, P. J. Ryan, J.-W. Kim, T. R. Paude, J.-H. Kang, J.W. Spinuzzi, D. A. Tenne, E. Y. Tsymba, M. S. Rzechowski, L. Q. Chen, J. Lee, and C. B. Eom, *Science* **362**, 1037 (2018).
- [31] K. Horiba, H. Ohguchi, H. Kumigashira, M. Oshima, K. Ono, N. Nagasawa, M. Lippmaa, M. Kawasaki, and H. Koinuma, *Rev. Sci. Instrum.* **74**, 3406 (2003).
- [32] E. Sakai, K. Yoshimatsu, K. Shibuya, H. Kumigashira, E. Ikenaga, M. Kawasaki, Y. Tokura, and M. Oshima, *Phys. Rev. B* **84**, 195132 (2011).
- [33] See Supplemental Material at [URL] for detailed characterizations of the measured samples, experimental conditions for spectroscopic measurements, probing depths of the present soft-x-ray spectroscopies, irradiation-time dependence of PES spectra, and thermal hysteresis in sheet resistance, which includes Refs. [34–39].
- [34] K. Shibuya, M. Kawasaki, and Y. Tokura, *Appl. Phys. Lett.* **96**, 022102 (2010).
- [35] J. C. Rakotoniaina, R. Mokrani-Tamellin, J. R. Gavarri, G. Vacquier, A. Casalot, and G. Calvarin, *J. Solid State Chem.* **103**, 81 (1993).
- [36] Y. Muraoka, H. Nagao, S. Katayama, T. Wakita, M. Hirai, T. Yokoya, H. Kumigashira, and M. Oshima, *Jpn. J. Appl. Phys.* **53**, 05FB09 (2014).
- [37] A. F. Santander-Syro, C. Bareille, F. Fortuna, O. Copie, M. Gabay, F. Bertran, A. Taleb-

- Ibrahimi, P. Le Fèvre, G. Herranz, N. Reyren, M. Bibes, A. Barthélémy, P. Lecoeur, J. Guevara, and M. J. Rozenberg, *Phys. Rev. B* **86**, 121107(R) (2012).
- [38] S. Moser, L. Moreschini, J. Jaćimović, O. S. Barišić, H. Berger, A. Magrez, Y. J. Chang, K. S. Kim, A. Bostwick, E. Rotenberg, L. Forró, and M. Grioni, *Phys. Rev. Lett.* **110**, 196403 (2013).
- [39] T. C. Rödel, F. Fortuna, F. Bertran, M. Gabay, M. J. Rozenberg, A. F. Santander-Syro, and P. Le Fèvre, *Phys. Rev. B* **92**, 041106(R) (2015).
- [40] Y. Muraoka and Z. Hiroi, *Appl. Phys. Lett.* **80**, 583 (2002).
- [41] J. W. Tashman, J. H. Lee, H. Paik, J. A. Moyer, R. Misra, J. A. Mundy, T. Spila, T. A. Merz, J. Schubert, D. A. Muller, P. Schiffer, and D. G. Schlom, *Appl. Phys. Lett.* **104**, 063104 (2014).
- [42] S. Shin, S. Suga, M. Taniguchi, M. Fujisawa, H. Kanzaki, A. Fujimori, H. Daimon, Y. Ueda, K. Kosuge, and S. Kachi, *Phys. Rev. B* **41**, 4993 (1990).
- [43] K. Okazaki, H. Wadati, A. Fujimori, M. Onoda, Y. Muraoka, and Z. Hiroi, *Phys. Rev. B* **69**, 165104 (2004).
- [44] R. Eguchi, M. Taguchi, M. Matsunami, K. Horiba, K. Yamamoto, A. Chainani, Y. Takata, M. Yabashi, D. Miwa, Y. Nishino, K. Tamasaku, T. Ishikawa, Y. Senba, H. Ohashi, I. H. Inoue, Y. Muraoka, Z. Hiroi, and S. Shin, *J. Electron Spectrosc. Relat. Phenom.* **156**, 421 (2007).
- [45] M. Abbate, F.M. F. de Groot, J. C. Fuggle, Y. J. Ma, C. T. Chen, F. Sette, A. Fujimori, Y. Ueda, and K. Kosuge, *Phys. Rev. B* **43**, 7263 (1991).
- [46] F. M. F. de Groot, *J. Electron Spectrosc. Relat. Phenom.* **67**, 529 (1994).
- [47] A. X. Gray, J. Jeong, N. P. Aetukuri, P. Granitzka, Z. Chen, R. Kukreja, D. Higley, T. Chase, A.H. Reid, H. Ohldag, M.A. Marcus, A. Scholl, A. T. Young, A. Doran, C. A. Jenkins, P. Shafer, E. Arenholz, M. G. Samant, S. S. P. Parkin, and H. A. Dürr, *Phys. Rev. Lett.* **116**, 116403 (2016).
- [48] M. K. Liu, M. Wagner, E. Abreu, S. Kittiwatanakul, A. McLeod, Z. Fei, M. Goldflam, S. Dai, M. M. Fogler, J. Lu, S. A. Wolf, R. D. Averitt, and D. N. Basov, *Phys. Rev. Lett.* **111**, 096602 (2013).
- [49] J. Laverock, S. Kittiwatanakul, A. A. Zakharov, Y. R. Niu, B. Chen, S. A. Wolf, J. W. Lu, and K. E. Smith, *Phys. Rev. Lett.* **113**, 216402 (2014).
- [50] M. Thees, M.-H. Lee, R. L. Bouwmeester, P. H. Rezende-Gonçalves, E. David, A. Zimmers, F. Fortuna, E. Frantzeskakis, N. M. Vargas, Y. Kalcheim, P. L. Fèvre, K. Horiba, H.

Kumigashira, S. Biermann, J. Trastoy, M. J. Rozenberg, I. K. Schuller, A. F. Santander-Syro, *Aci. Adv.* **7**, eabj1164 (2021).

[51] X. Tan, T. Yao, R. Long, Z. Sun, Y. Feng, H. Cheng, X. Yuan, W. Zhang, Q. Liu, C. Wu, Y. Xie, and S. Wei, *Sci. Rep.* **2**, 466 (2012).

[52] C. H. Griffiths and H. K. Eastwood, *J. Appl. Phys.* **45**, 2201 (1974).

Supplemental Material

***In situ* photoemission study of collective electronic phase transition in VO₂-based heterostructures**

D. Shiga^{1,2,*}, S. Inoue¹, T. Kanda¹, N. Hasegawa¹, M. Kitamura², K. Horiba², K. Yoshimatsu¹,
A. F. Santander-Syro³, and H. Kumigashira^{1,2,*}

¹ *Institute of Multidisciplinary Research for Advanced Materials (IMRAM), Tohoku University, Sendai 980–8577, Japan*

² *Photon Factory, Institute of Materials Structure Science, High Energy Accelerator Research Organization (KEK), Tsukuba 305–0801, Japan*

³ *Institut des Sciences Moléculaires d'Orsay, Université Paris-Saclay, 91405 Orsay, France*

*Correspondence authors: dshiga@tohoku.ac.jp, kumigashira@tohoku.ac.jp

S1. Sample characterization

A. Surface morphology

The atomically flat surfaces of all the measured samples — 9-nm VO₂ and V_{0.99}W_{0.01}O₂ (W:VO₂) single-layer films and VO₂ (4.5 nm)/W:VO₂ (4.5 nm) bilayer structures grown on TiO₂ (001) substrates — were confirmed by *ex situ* atomic force microscopy (AFM). The typical AFM images are shown in Fig. S1. The AFM images show similar surface morphologies. The root-mean-square roughness R_{rms} estimated from the AFM images is all less than 0.2 nm. The values are almost the same as that of the original TiO₂ substrate ($R_{\text{rms}} = 0.16$ nm). The R_{rms} values of the measured films were all less than the V-V dimer length (approximately 0.3 nm), indicating that these films were controlled to the scale of the V-V dimer length and that the smooth surface and interface were maintained not only in the single-layer films but also in the bilayer structures.

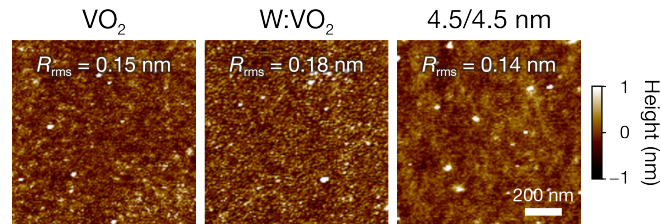


Fig. S1. Typical AFM images of the measured 9-nm VO₂ single-layer films, 9-nm W:VO₂ single-layer films, and VO₂ (4.5 nm)/W:VO₂ (4.5 nm) bilayer structures grown on TiO₂ (001) substrates.

B. Crystal structure

The crystal structures of the 9-nm VO₂ and V_{0.99}W_{0.01}O₂ (W:VO₂) single-layer films and the VO₂ (4.5 nm)/W:VO₂ (4.5 nm) bilayer structures were characterized by x-ray diffraction (XRD) measurements, which confirmed the achievement of single phase in both the single-layer films and the absence of another phase in the bilayer, as well as their coherent growth on TiO₂ (001) substrates. Figure S2(a) shows the out-of-plane XRD patterns around the (002)_R reflection for the films and bilayer. The formation of single phase for the films and the absence of another phase in the bilayer are confirmed. In addition, the presence of well-defined Laue fringes indicates the formation of atomically flat surfaces and chemically abrupt interface. The estimated out-of-plane lattice constant (c_R) of the VO₂ and W:VO₂ films are 0.2829(4) nm and

0.2839(4) nm, respectively. These values are in good agreement with previous reports [34], guaranteeing the high quality of the present samples. The XRD pattern for the bilayer is well fitted with a two-layer model consisting of a VO₂ layer [$c_R = 0.2829(4)$] nm and a W:VO₂ layer [$c_R = 0.2839(4)$] nm, indicating the formation of a chemically abrupt heterointerface between the two layers, as well as between the layer and the substrate, as reported previously [29]. The coherent growth of the bilayer on TiO₂ (001) substrates is confirmed by the reciprocal space mapping (RSM) around the (112)_R reciprocal point, as well as the absence of another phase, as shown in Fig. S2(b). As shown in Fig. S2(b), the in-plane lattice constant of the layers remains pinned to that of the TiO₂ substrate, indicating the coherent growth of the bilayer. These crystallographic results identify the present films and bilayers as being highly crystalline.

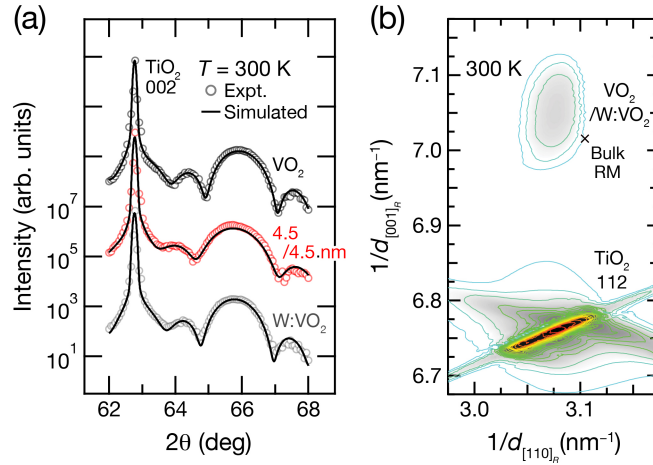


Fig. S2. (a) Typical out-of-plane XRD patterns around the (002)_R reflection measured at room temperature for 9-nm VO₂ and W:VO₂ single-layer films and VO₂ (4.5 nm)/W:VO₂ (4.5 nm) bilayers grown on TiO₂ (001) substrates. Simulated XRD patterns based on corresponding single- or two-layer models (black curves) are overlaid. (b) RSM around the (112)_R reciprocal point for the bilayer. The cross mark denotes lattice constants of bulk VO₂ in the rutile-metallic (RM) phase [35] for reference.

S2. Experimental geometry in polarization-dependent x-ray absorption measurement

Figure S3 depicts the schematic of our experimental geometry for *in situ* polarization-dependent x-ray absorption spectroscopy (XAS) measurements, including the crystal axes of a $\text{VO}_2(001)_R$ film sample and the polarization vector \mathbf{E} . Regarding linear dichroism measurements for XAS, we acquired the spectra at angles $\theta = 0^\circ$ and 60° between \mathbf{E} and the a_R -axis direction, which is defined as the a -axis direction in the rutile structure ($[100]_R$), while maintaining a fixed angle of 60° between the direction normal to the $(001)_R$ surface and the incident light. The maintenance of the fixed angle between the direction normal to the surface and the incident light ensures that the probing depth corresponding to the two spectra with different θ values is the same. In the present experimental geometry, XAS spectra with $\mathbf{E} \parallel c_R$ (I_{\parallel}) can be deduced from the expression $I_{\parallel} = (4/3)(I - I_{\perp}/4)$, where I and I_{\perp} (namely, that corresponding to $\mathbf{E} \perp c_R$) denote XAS spectra measured with grazing ($\theta = 60^\circ$) and normal ($\theta = 0^\circ$) incidences, respectively.

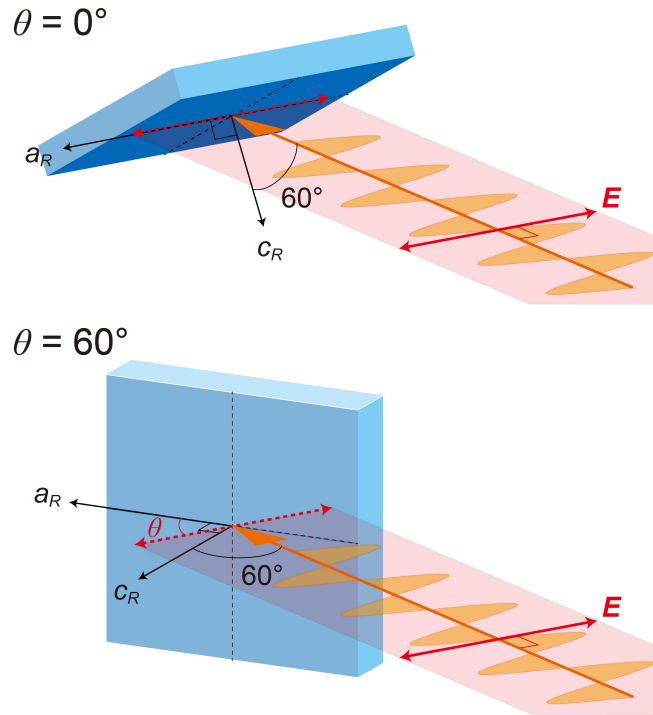


Fig. S3. Schematic of our experimental geometry of polarization-dependent XAS measurements of a $\text{VO}_2(001)_R$ film at $\theta = 0^\circ$ and 60° . The a_R - and c_R -axis directions are defined as the a - and c -axis directions in the rutile structure, respectively.

S3. Probing depths of the present soft-x-ray spectroscopies

To evaluate the probing depth of photoemission spectroscopy (PES) λ^{PES} and x-ray absorption spectroscopy (XAS) λ^{XAS} , we measured the overlayer-thickness dependence of Ti $2p$ core-level spectra and Ti L_3 -edge XAS for VO₂/Nb:TiO₂ (001) single-layer films, as shown in Figs. S4(a) and S4(b), respectively. Each spectrum is normalized to the incident photon flux; hence, the observed intensity reduction with increasing VO₂ overlayer thickness t reflects the attenuation of the Ti-derived signal from buried TiO₂ substrates by the VO₂ overlayer. For both the soft-x-ray (SX) spectroscopies, the intensity decreases steeply with increasing t and becomes almost undetectable at $t = 3$ nm, highlighting the surface sensitivity of the two spectroscopic measurements, as well as the formation of the chemically abrupt interface between the VO₂ layer and TiO₂ substrate [15]. To evaluate the probing depths for PES and XAS, we plot the Ti $2p$ core-level intensity $I_{\text{Ti}2p}^{\text{PES}}$ and Ti L_3 XAS intensity $I_{\text{Ti}2p}^{\text{XAS}}$ as a function of t in Fig. S4(c) and fit them by attenuation functions of $I_{\text{Ti}2p}^{\text{PES}} = e^{-t/\lambda^{\text{PES}}}$ for PES and $I_{\text{Ti}2p}^{\text{XAS}} = e^{-t/\lambda^{\text{XAS}}}$ for XAS, respectively. As shown in Fig. S4(c), the intensity reductions are well fitted to the attenuation functions with $\lambda^{\text{PES}} = 0.55(2)$ and $\lambda^{\text{XAS}} = 0.70(1)$. The similar values of λ^{PES} and λ^{XAS} indicate that both SX spectroscopies probe approximately the same region. Based on these values, the signal contributions from the upper 4.5-nm-thick VO₂ layer in the present PES and XAS measurements are estimated to be 99.97% and 99.84%, respectively. These results indicate that both PES and XAS measurements predominantly probe the upper VO₂ layer of bilayer structures.

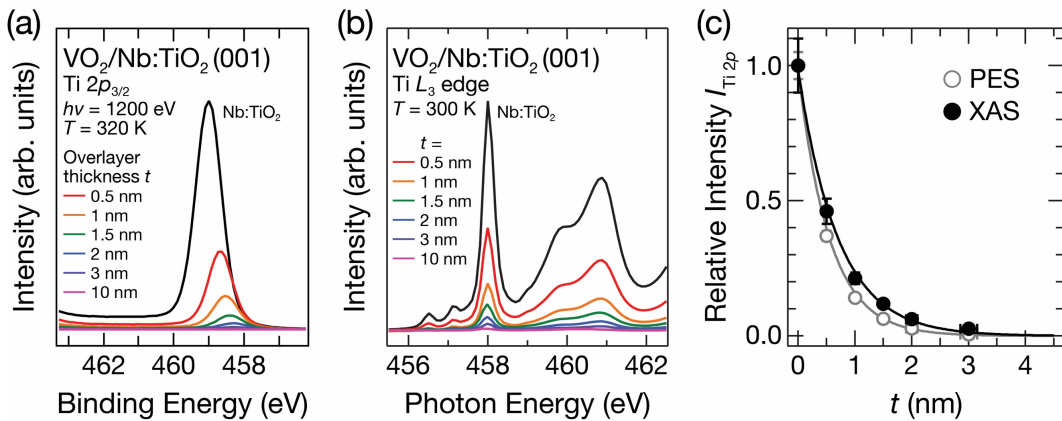


Fig. S4. (a) Ti $2p_{3/2}$ core-level spectra [15] and (b) Ti L_3 XAS spectra for VO₂/Nb:TiO₂ (001) single-layer films with varying t , along with that of the Nb:TiO₂ substrate as reference. (c) Relative intensities of the Ti $2p_{3/2}$ core-level PES spectra ($I_{\text{Ti}2p}^{\text{PES}}$, gray open circles) and Ti L_3 XAS

spectra ($I_{\text{Ti}2p}^{\text{XAS}}$, black solid circles), plotted as functions of t . Gray and black curves represent fits using attenuation models with $\lambda^{\text{PES}} = 0.55(2)$ nm and $\lambda^{\text{XAS}} = 0.70(1)$ nm, respectively.

S4. Irradiation-time dependence of valence band spectra

It is well known that VO_2 exhibits an insulator-to-metal transition upon irradiation by soft-x-ray (SX) [36]. Therefore, to perform the photoelectron spectroscopic measurements within a period in which no detectable spectral changes due to SX irradiation are observed, we measured the irradiation-time dependence of the valence-band spectra for insulating VO_2 , as shown in Fig. S5. No detectable spectral differences near the Fermi level (E_F) are observed between the spectra acquired before (initial) and after 15 minutes of SX irradiation, whereas certain slight changes are detectable in the spectra after 45 minutes. Therefore, we changed the location of the light spot on each sample every 15 minutes during the present measurements. All the PES and XAS spectra shown in the text and Supplemental Material were acquired within this period. Thus, the light irradiation effects are negligible in the present study.

As shown in Fig. S5, the intensity (area under the curve) of the O $2p$ bands decreases after 45 minutes of SX irradiation in parallel with the broadening of the V $3d$ band near E_F , whereas the area under the curve for the V $3d$ band remains unchanged. This indicates that the changes in the V $3d$ spectra near E_F might originate from oxygen vacancies generated by SX irradiation, as observed in many transition metal oxide systems [36–39].

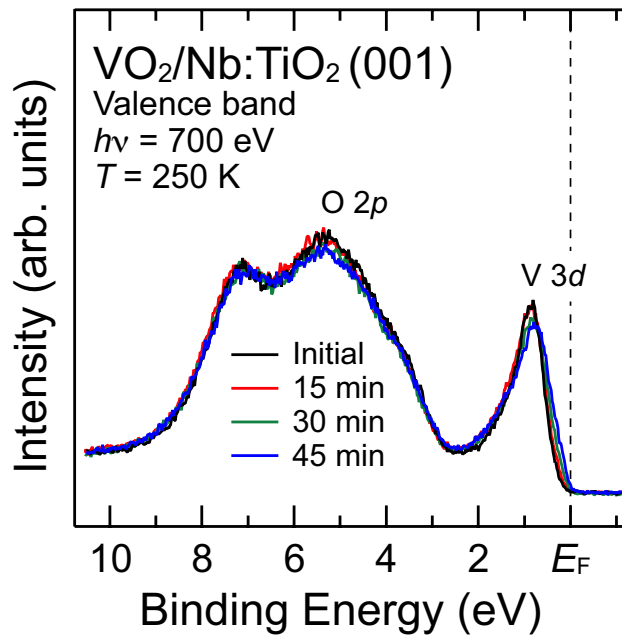


Fig. S5. Irradiation-time dependence of valence-band spectra for $\text{VO}_2/\text{Nb:TiO}_2(001)$ films.

S5. Thermal hysteresis in sheet resistance

Figure S6 shows the temperature dependence of the sheet resistance R_{Sheet} for VO_2 (4.5 nm)/ W:VO_2 (4.5 nm) bilayers, along with 9-nm epitaxial VO_2 and W:VO_2 single-layer films. Note that the $R_{\text{Sheet}}-T$ curves measured upon cooling are the same as those in Fig. 2 in the main text. The hysteresis loop characteristic of a first-order transition in VO_2 films is clearly observed for the bilayer. The hysteresis loops almost close at 300 K. Therefore, to avoid the possible hysteresis effects in the present spectroscopic measurements, the sample temperature was maintained at 320 K for half an hour prior to the spectroscopic measurements, and then all spectroscopic data were acquired only during cooling.

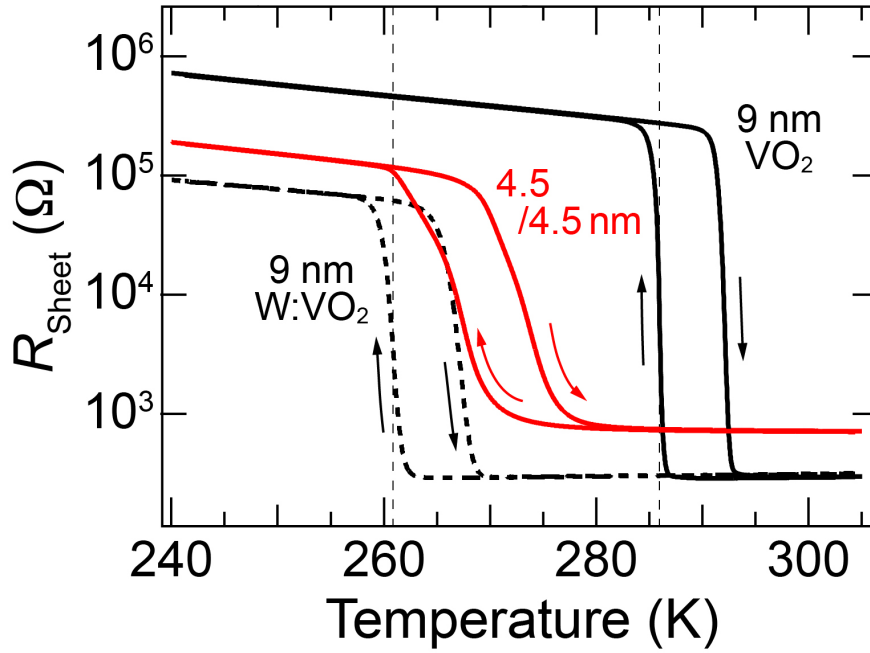


Fig. S6. Temperature dependence of R_{Sheet} for VO_2 (4.5 nm)/ W:VO_2 (4.5 nm) bilayer (solid red curve) and 9-nm epitaxial VO_2 and W:VO_2 single-layer films (solid and dashed black curves, respectively) grown on TiO_2 (001) substrates. Vertical dashed lines indicate $T_{\text{MIT}}^{\text{Cooling}}$ of the VO_2 (286 K) and electron-doped W:VO_2 (261 K) single-layer films.